SPE-173235-MS

Identifiability of Location and Magnitude of Flow Barriers in Slightly Compressible Flow

S. Kahrobaei, M. Mansoori, and J.D. Jansen, Delft University of Technology, The Netherlands; G.J.P. Joosten, Shell Global Solutions International B.V., Rijswijk, The Netherlands; P.M.J. Van den Hof, Eindhoven University of Technology, The Netherlands

This paper was prepared for presentation at the SPE Reservoir Simulation Symposium held in Houston, Texas, USA, 23–25 February 2015.

Abstract

Classic identifiability analysis of flow barriers in incompressible single-phase flow reveals that it is not possible to identify the location and permeability of low-permeable barriers from production data (well bore pressures and rates), and that only averaged reservoir properties in-between wells can be identified. We extend the classic analysis by including compressibility effects. We use two approaches: 1) a twin-experiment with synthetic production data for use with a time-domain parameter estimation technique, and 2) a transfer function formalism in the form of bilaterally coupled four-ports allowing for an analysis in the frequency domain. We investigate the identifiability, from noisy production data, of the location and the magnitude of a low-permeable barrier to slightly-compressible flow in a one-dimensional configuration. We use an unregularized adjoint-based optimization scheme for the numerical time-domain estimation, using various levels of sensor noise, and confirm the results using the semi-analytical transfer function approach. Both the numerical and semi-analytical results show that it is possible to identify the location and the magnitude of the permeability in the barrier from noise-free data. By introducing increasingly higher noise levels the identifiability gradually deteriorates, but the location of the barrier remains identifiable for much higher noise levels than the permeability. The shape of the objective function surface, in normalized variables, indeed indicates a much higher sensitivity of the well data to the location of the barrier than to its magnitude. These theoretical results appear to support the empirical finding that unregularized gradient-based history matching in large reservoir models, which is well known to be a severely ill-posed problem, occasionally leads to useful results in the form of model parameter updates having unrealistic magnitudes but indicating the correct location of model deficiencies.

Introduction

Estimating reservoir parameters from measured data is an ill-posed inverse problem due to the large number of parameters and the limited available data (Shah et al., 1978; Oliver et al., 2008). Consequently, it is important to understand which parameters can be estimated with reasonable accuracy from the available data. This aspect can be addressed as determining the identifiability of parameters.

From a systems and control theory perspective, the transient response of a dynamic system contains information about dynamics-related properties of a system. Consequently, including compressibility effects (leading to a transient response) can result in a more accurate reservoir parameter estimation than just considering the steady-state response. The pressure behavior of a slightly-compressible single-phase fluid in a reservoir can be described accurately by the diffusivity equation. Theoretically, the pressure response of every point in a reservoir to e.g. step or impulse inputs, which cause transient behavior, contains the information about reservoir boundaries and reservoir heterogeneities (Grader and Horne, 1988; Van Doren, 2010). However certain parameters have a more significant effect on this transient response than others. Subsequently, by investigating the effect of different parameters on the dynamic behavior we can understand which parameters are more identifiable from the available data. On the other hand, presence of noise in the data may smear the identifiability of such parameters and can result in unrealistic parameter estimates (Dogru et al., 1977). Hence, it is important to also investigate the effect of noise on identifiability of different parameters.

Identifiability of reservoir heterogeneity has been studied by several authors (Stallman, 1952; Watson et al., 1984; Yaxley, 1987; Grader and Horne, 1988; Van Doren et al., 2008; Zandvliet et al., 2008; Ahn and Horne, 2010; Van Doren, 2010). The concept of identifiability as used in systems and control theory can loosely be defined as the capacity to infer the magnitude of model parameters from given input and output data. For a more precise, mathematical definition of identifiability as applied to porous media flow, see Van Doren (2010). Stallman (1952) analyzed the pressure response of a constant-rate well and presented a log-log type curves for constant pressure boundaries as well as impermeable linear boundaries. Watson et al. (1984) investigated the identifiability of estimates of two-phase reservoir properties in history matching. They concluded that for single-phase incompressible flow, only the harmonic average of the permeability distribution is identifiable and subsequently the presence of the saturation distribution is essential to identify the absolute permeability spatial distribution. Yaxley (1987) investigated the effects of a partially communicating linear fault on transient pressure behavior. Grader and Horne (1988) and Ahn and Horne (2010) considered (slightly) compressible flow and used well testing related methods such as interference testing and pulse testing to investigate the detectability of reservoir heterogeneities. They showed that there is sometimes information about the distance between wells and flow-relevant features (e.g. reservoir boundaries, impermeable subregions or permeability distribution) in the data, although to a limited extent due to the diffusive nature of pressure transients.

The objective of this paper is to investigate the identifiability of location and magnitude of a flow barrier in compressible single-phase flow by analyzing the effect of this heterogeneity on dynamical behavior of the flow. The motivation stems from a paper by Joosten et al. (2011) who showed that sometimes the application of unregularized reservoir parameter estimation still appears to have added value. They argued, based on numerical examples, that localized unrealistic parameter values can be used as an indicator of model errors in the underlying reservoir model. In a follow-up study, Kahrobaei et al. (2014) showed that the application of unregularized reservoir parameter estimation may sometimes indeed give an indication of the location of significant missing features in the model. In the present study we further analyze this phenomenon by addressing the identifiability of flow-relevant features. In particular, we apply two approaches to study the possibility of detecting a low-permeable barrier from the observations (outputs of the system). In the first approach we conduct three different twin-experiments with synthetic production data contaminated with different noise levels in the time domain. In our twin experiments an unregularized parameter estimation is applied to update uncertain parameters (grid block permeabilities) in a one-dimensional (1D) reservoir model that contains a major deficiency in the form of a missing low permeability feature. In the second approach we develop an analytical method to explain our time-domain findings. In this approach we consider flow through porous media as a linear system and develop a method that gives an analytical expression for the dynamic characteristics of the system as a function of the system's geometric properties, heterogeneity etc. in the frequency domain. This solution

Figure 1—Permeability field of a one-dimensional homogenous reservoir model with a low-permeable barrier. The blue and orange dots indicate the injector and the producer respectively.

Figure 2—Permeability field of the starting model. The blue and orange dots indicate the injector and the producer respectively.

is obtained based on a transfer function formalism applied to a series of bilaterally coupled porous media models.

The structure of this paper is as follows: in section 2 we present and discuss the numerical twin-experiment results in the time-domain. The transfer function formulation is derived in section 3. In section 4 we investigate effects of location and magnitude of a flow barrier on the output of a system. Subsequently, in section 5 we present and discuss the parameter estimation results based on frequency responses of the system. In section 6 the objective function space is visualized and the parameter identifiability is discussed. We end the paper with a brief discussion and conclusions.

Time-Domain Twin Experiments

We perform three 'twin experiments'. They all use the same 'truth model' to generate synthetic data, but the resulting data are contaminated with different noise levels. The first experiment involves the assimilation of noise-free production data, while in the last two experiments we assimilate noisy production data.

Synthetic Truth

Consider one-dimensional single-phase flow of a slightly compressible fluid through a porous medium. The domain has a homogenous permeability distribution with a low permeable barrier in between. The size of the reservoir is 500m × 50m × 2m, which is divided into 50 grid blocks. The reservoir is produced with an injector at the left side and a producer at the right side. A low-permeable barrier with a width of 30 m, is located at 350 m from the injector. The background permeability is 300 mD and the permeability of the barrier is 0.1 mD. The reservoir has a uniform porosity of 0.2. The initial pressure is 300 MPa. The producer is operating at a bottom hole pressure of 250 MPa and the injector at a constant flow rate of 0.002 m^3/s. The reservoir is simulated for 1000 days and we measure the flow rates in the producer on a daily basis. Figure 1 shows the permeability field of the reservoir with its low permeable barrier.

Starting Reservoir Model

The low-permeable barrier in the reservoir is missing in the starting model. All remaining parameters in the starting model are identical to those of the 'truth' case. Figure 2 depicts the uniform permeability field of the starting model with a constant permeability of 300 mD.

For parameter estimation purposes we try to minimize an objective function, which is defined as a mismatch between observed data and simulated data:

$$J(\mathbf{m}) = \left(\mathbf{d} - \mathbf{y}(\mathbf{m})\right)^T \mathbf{P}_d^{-1} \left(\mathbf{d} - \mathbf{y}(\mathbf{m})\right), \tag{1}$$

where $\mathbf{m}$ is a vector of unknown model parameters (grid block permeabilities for the present study), $\mathbf{d}$ is a vector of data (measurements), $\mathbf{y}$ is a vector valued-function that relates the model parameters to the model outputs (i.e. the simulated data), and $\mathbf{P}_d$ is a square positive semi-definite matrix of weight factors which is chosen as the measurement error covariance matrix. Minimization of the objective function is achieved by adjustment of the model parameters $\mathbf{m}$. Various numerical techniques are available

Figure 3—Updated permeability field of the 1D reservoir model for experiment #1.

Table 1—Grid block numbers and permeabilities of the low permeable barrier in the 'truth' and the updated model.

Model	Grid block No.	Permeability value [mD]
Truth parameters	36	0.1
	37	0.1
	38	0.1
Updated parameters	36	0.1
	37	0.0997
	38	0.1

Figure 4—Updated permeability field of the 1D reservoir model for experiment #2.

to perform this minimization, the most efficient one being gradient-based minimization where the gradient is computed using the adjoint method (Oliver et al., 2008). For the present study we used an in-house reservoir simulator with adjoint-functionality and an iterative gradient-based minimization procedure (Kraaijevanger et al., 2007)

Experiment #1: Parameter Estimation Based on Noise-Free Measurements

In the first twin experiment, parameter estimation is performed starting from the uniform reservoir model, depicted in Figure 2, based on perfect (noise-free) production data. Figure 3 shows the updated permeability field after parameter estimation.

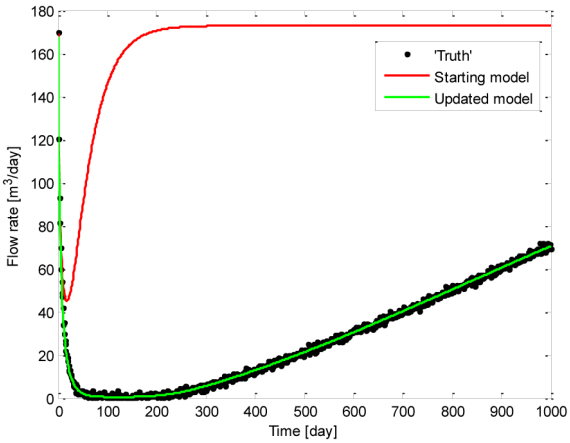

Figure 5—Production profile for truth, starting and updated model in experiment #2.

Table 1 lists the grid block numbers and corresponding permeability values of the low permeable barrier in the 'truth' case and the updated model (Figure 1 and Figure 3 respectively).

As can be seen in Table 1, the grid block numbers and the grid block permeabilities of the low permeable barrier in the updated model are exactly the same as those in the 'truth' case.

Experiment #2: Parameter Estimation Based on Noisy Measurements: High Signal to Noise Ratio

In second twin experiment parameter estimation is performed starting from the same reservoir model as experiment #1 but based on noisy production data. Errors are generated by sampling from a Gaussian distribution with zero mean and a standard deviation equal to 1 m^3/day. Negative production rates, after the addition of noise, are reset to zero. It is assumed that the measurements were affected by independent noise, which results in a diagonal covariance matrix for the observation errors. Figure 4 depicts the updated permeability field after parameter estimation based on noisy data (with known covariance). Figure 5 shows the production profile for truth, starting and updated models.

Table 2—Grid block numbers and permeabilities of the low permeable barrier in the 'truth' and the updated model.

Model	Grid block No.	Permeability value [mD]
Truth parameters	36	0.1
	37	0.1
	38	0.1
Updated parameters	36	0.1036
	37	0.1206
	38	0.08

Figure 6—Updated permeability field of the 1D reservoir model for experiment #3.

Table 2 lists the grid block numbers and corresponding permeability values of the low permeable barrier in the 'truth' case and the updated model for experiment #2.

As can be seen in Table 2, in the experiment with noisy measurements the positions of the low-permeable barriers in the 'truth' case and the updated model are exactly the same but the permeability value of the corresponding grid blocks in the updated model are not as accurate as those obtained in the noise-free experiment.

Experiment #3: Parameter Estimation Based on Noisy Measurements: Low Signal to Noise Ratio

In the third twin experiment the amount of error in the data is increased in comparison with experiment #2. In this case, the errors are generated from a Gaussian distribution with zero mean and a standard deviation equal to 10 m^3/day. Figure 6 depicts the updated permeability field of the 1D reservoir model after parameter estimation. Figure 7 depicts the production profile for truth, starting and updated models.

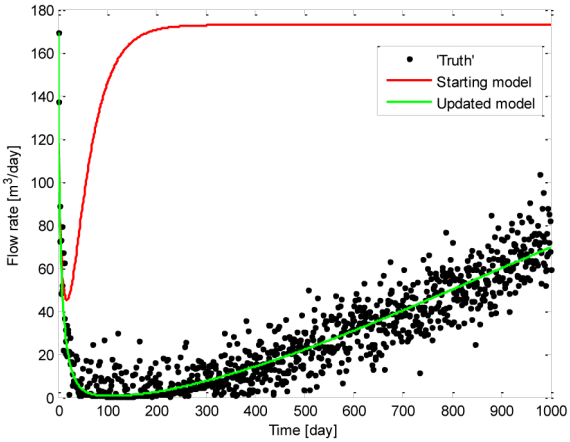

Figure 7—Production profile for truth, starting and updated model in experiment #3.

Table 3—Grid block number and grid block permeability of the low permeable barrier in the truth and updated model

Model	Grid block No.	Permeability value [mD]
Truth parameters	36	0.1
	37	0.1
	38	0.1
Updated parameters	36	0.026
	37	19.15
	38	89.6

Table 3 lists the grid block numbers and corresponding permeability values of the low permeable barrier in the 'truth' case and the updated model for experiment #3.

As can be seen in Table 3, by increasing the noise level in the measurements, the positions of the grid blocks with the lowest permeabilities in the updated model and the truth case are still identical, but the permeability values of those grid blocks are now significantly different.

We note that the deviation of our estimates from the true values is caused by random noise in the measurements. Different realizations of the measurement noise will therefore result in different deviations of the estimates.

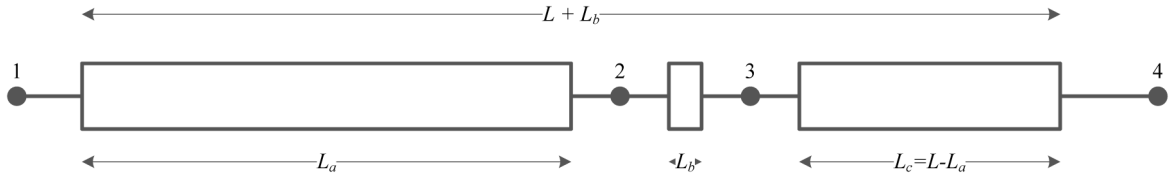

Figure 8—Schematic representation of two one-dimensional domains separated by a low permeable barrier.

Transfer Function Representation

To further analyze the behavior that was observed in our 1D twin-experiments in the time-domain, we conduct 1D experiments using a transfer function formalism to characterize the identifiability of the location and magnitude of model deficiencies (absence of flow barriers). We use a two-port network approach which results in a lumped-parameter representation of our system. The structure of the 1D initial-boundary value problem allows for the input to output representation of the system in terms of pressure and flow rate at two points in the spatial domain, mapped by a linear transformation.

Model Description

The 1D reservoir model that was described in Section 2 can be considered as a system that consists of three blocks. The total length of the domain and the length of the middle block are known. The length of the first block of the domain is unknown, resulting in an unknown position of the middle block. Note that length of the third block is a function of the length of the first block, since the total length of the domain is constant. The middle block works as a barrier to flow from point 1 to point 4; see Figure 8.

Governing Equations

The pressure behavior of a slightly-compressible single-phase fluid in a reservoir can be described by the diffusivity equation. The pressure diffusion equation for linear flow between two points can therefore be written as:

$$\frac{\partial p(x,t)}{\partial t} = \eta \frac{\partial^2 p(x,t)}{\partial x^2}, \tag{2}$$

in which η is defined as hydraulic diffusivity:

$$\eta = \frac{k}{\varphi \mu c_t}, \tag{3}$$

where k is permeability, φ is porosity, μ is viscosity and c_t is total compressibility. Moreover, the flow rate for linear flow between two points can be written as:

$$q(x,t) = -A \frac{k}{\mu} \frac{\partial p(x,t)}{\partial x}, \tag{4}$$

where A is the surface area.

Dimensionless Variables

To transform equation (2) and equation (4) into dimensionless equations, the following dimensionless variables are defined:

– Dimensionless length

$$\xi = \frac{x}{L}, \tag{5}$$

where L is total constant length of the first and the last blocks of Figure 8.

– Dimensionless pressure

$$\pi = \frac{p}{\hat{p}}, \tag{6}$$

where $\hat{p}$ is pressure at the outlet boundary.

– Dimensionless time

$$\tau = \frac{kt}{\mu c_t \varphi L^2}. \tag{7}$$

Using these dimensionless variables, we can rewrite equations (2) and (4) in dimensionless form:

$$\frac{\partial \pi}{\partial \tau} = \frac{\partial^2 \pi}{\partial \xi^2}, \tag{8}$$

$$\theta = -\alpha \frac{\partial \pi}{\partial \xi}, \tag{9}$$

where α is a dimensionless number defined as

$$\alpha = \frac{Ak\hat{p}}{L\mu\hat{q}}, \tag{10}$$

in which $\hat{q}$ is the flow rate at the inlet boundary.

Transfer Function Derivation

In order to find input-output relations of the system depicted in Figure 8, first the transfer functions of each block are derived and then they are coupled together to obtain transfer functions that describe the entire system.

Input-Output Relations of One Block of the System By applying a Laplace transform to the equation (8) we obtain

$$\frac{\partial^2}{\partial \xi^2} \Pi(\xi, s) - s\Pi(\xi, s) = 0. \tag{11}$$

Equation (11) has a solution of the form

$$\Pi(\xi, s) = C_1 e^{\xi\sqrt{s}} + C_2 e^{-\xi\sqrt{s}}. \tag{12}$$

Moreover, equation (9) can also be written in the Laplace domain as follows:

$$\Theta(\xi, s) = -\alpha C_1 \sqrt{s} e^{\xi\sqrt{s}} + \alpha C_2 \sqrt{s} e^{-\xi\sqrt{s}}, \tag{13}$$

where functions C_1 and C_2 can be determined by requiring the solution to satisfy the boundary conditions: $\Theta(\xi, s) = \Theta(\xi_1, s)$ at $\xi = \xi_1$ and $\Pi(\xi, s) = \Pi(\xi_2, s)$ at $\xi = \xi_2$. Consequently, solving for C_1 and C_2 leads to:

$$C_1 = \frac{1}{\Lambda(s) + \Lambda^{-1}(s)} \Pi(\xi_2, s) - \frac{1}{\alpha\sqrt{s}} \frac{\Lambda^{-1}(s)}{\Lambda(s) + \Lambda^{-1}(s)} \Theta(\xi_1, s), \tag{14}$$

$$C_2 = \frac{1}{\Lambda(s) + \Lambda^{-1}(s)} \Pi(\xi_2, s) + \frac{1}{\alpha\sqrt{s}} \frac{\Lambda(s)}{\Lambda(s) + \Lambda^{-1}(s)} \Theta(\xi_1, s), \tag{15}$$

in which

$$\Lambda(s) = e^{\xi_2\sqrt{s}}. \tag{16}$$

At the boundaries we have the following output variables:

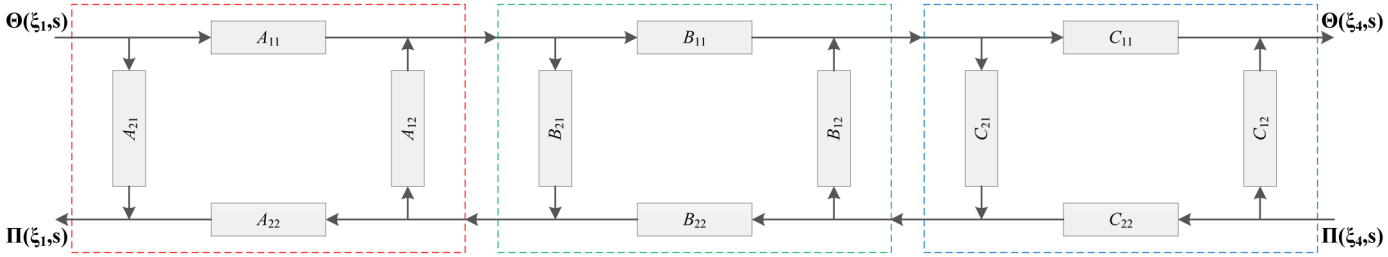

Figure 9—Coupled model in block diagram representation for the model depicted in Figure 8.

$$\Pi(\xi_1,s)=C_1+C_2, \tag{17}$$

$$\Theta(\xi_2,s)=-\alpha C_1\sqrt{s}\Lambda(s)+\alpha C_2\sqrt{s}\Lambda^{-1}(s). \tag{18}$$

Inserting values of C_1 and C_2 from equations (14) and (15) in equations (17) and (18) gives the final solutions:

$$\Pi(\xi_1,s)=\frac{2}{\Lambda(s)+\Lambda^{-1}(s)}\Pi(\xi_2,s)+\frac{1}{\alpha\sqrt{s}}\frac{\Lambda(s)-\Lambda^{-1}(s)}{\Lambda(s)+\Lambda^{-1}(s)}\Theta(\xi_1,s), \tag{19}$$

$$\Theta(\xi_2,s)=\alpha\sqrt{z}\frac{\Lambda^{-1}(s)-\Lambda(s)}{\Lambda(s)+\Lambda^{-1}(s)}\Pi(\xi_2,s)+\frac{2}{\Lambda(s)+\Lambda^{-1}(s)}\Theta(\xi_1,s). \tag{20}$$

Subsequently $\Theta(\xi_2, s)$ and $\Pi(\xi_1, s)$ can be written as a function of the boundary conditions:

$$\begin{bmatrix}\Theta(\xi_2,s)\\ \Pi(\xi_1,s)\end{bmatrix}=\begin{bmatrix}A_{11} & A_{12}\\ A_{21} & A_{22}\end{bmatrix}\begin{bmatrix}\Theta(\xi_1,s)\\ \Pi(\xi_2,s)\end{bmatrix} \tag{21}$$

where A_{ij} are the transfer functions of the first block, which explain the input-output relations as a function of model parameters. These transfer functions can be derived as

$$A_{11}=\frac{2}{e^{\xi_2\sqrt{s}}+e^{-\xi_2\sqrt{s}}}=\frac{1}{\cosh\left(\xi_2\sqrt{s}\right)}, \tag{22}$$

$$A_{12}=\alpha\sqrt{s}\frac{e^{-\xi_2\sqrt{s}}-e^{\xi_2\sqrt{s}}}{e^{\xi_2\sqrt{s}}+e^{-\xi_2\sqrt{s}}}=-\alpha\sqrt{s}\tanh\left(\xi_2\sqrt{s}\right), \tag{23}$$

$$A_{21}=\frac{1}{\alpha\sqrt{s}}\frac{e^{\xi_2\sqrt{s}}-e^{-\xi_2\sqrt{s}}}{e^{\xi_2\sqrt{s}}+e^{-\xi_2\sqrt{s}}}=\frac{1}{\alpha\sqrt{s}}\tanh\left(\xi_2\sqrt{s}\right), \tag{24}$$

$$A_{22}=\frac{2}{e^{\xi_2\sqrt{s}}+e^{-\xi_2\sqrt{s}}}=\frac{1}{\cosh\left(\xi_2\sqrt{s}\right)}. \tag{25}$$

In this way we can derive the transfer functions for each block of our system.

Input-Output Relations of the Entire System By coupling the transfer functions of the three blocks we can derive the input-output relations for the entire system. Figure 9 depicts the coupled model in block diagram representation for our 1D reservoir model, where we used the letters A, B and C to indicate the three consecutive blocks of Figure 8.

Each block of Figure 9 has an input-output relation in the form of equation (21). Consequently, by performing matrix multiplications, we can find the transfer functions that represent the input-output relations for the entire system. The matrix form of the input-output relations can be written as

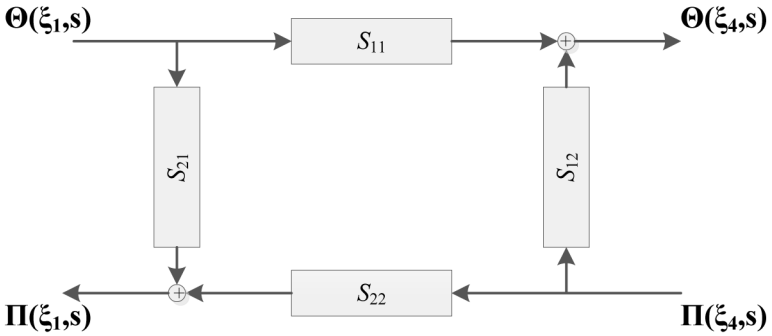

Figure 10—Modified block diagram representation for the model depicted in Figure 8.

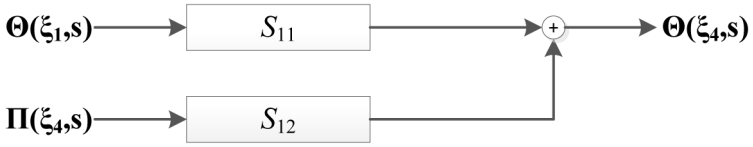

Figure 11—Input-output relation in the reservoir system.

$$\begin{bmatrix}\Theta(\xi_4,s)\\ \Pi(\xi_1,s)\end{bmatrix}=\begin{bmatrix}S_{11} & S_{12}\\ S_{21} & S_{22}\end{bmatrix}\begin{bmatrix}\Theta(\xi_1,s)\\ \Pi(\xi_4,s)\end{bmatrix}, \tag{26}$$

where the elements *Sij* are given by

$$S_{11}=-\frac{A_{11}A_{11}C_{11}}{C_{21}\left(B_{12}+A_{12}B_{11}B_{22}-A_{12}B_{12}B_{21}\right)+A_{12}B_{21}-1}, \tag{27}$$

$$S_{12}=-\frac{C_{12}-A_{12}C_{12}B_{21}+C_{11}C_{22}B_{12}-C_{12}C_{21}B_{12}+A_{12}C_{11}C_{22}B_{11}B_{22}-A_{12}C_{11}C_{22}B_{12}B_{21}-A_{12}C_{12}C_{21}B_{11}B_{22}+A_{12}C_{12}C_{21}B_{12}B_{21}}{A_{12}B_{21}+C_{21}B_{12}+A_{12}C_{21}B_{11}B_{22}-A_{12}C_{21}B_{12}B_{21}-1}, \tag{28}$$

$$S_{21}=-\frac{A_{21}+A_{11}A_{22}B_{21}-A_{12}A_{21}B_{21}-A_{21}C_{21}B_{12}+A_{11}A_{22}C_{21}B_{11}B_{22}-A_{11}A_{22}C_{21}B_{12}B_{21}-A_{12}A_{21}C_{21}B_{11}B_{22}+A_{12}A_{21}C_{21}B_{12}B_{21}}{A_{12}B_{21}+C_{21}B_{12}+A_{12}C_{21}B_{11}B_{22}-A_{12}C_{21}B_{12}B_{21}-1}, \tag{29}$$

$$S_{22}=-\frac{A_{22}C_{22}B_{22}}{A_{12}\left(B_{21}+C_{21}B_{11}B_{22}-C_{21}B_{12}B_{21}\right)+C_{21}B_{12}-1}, \tag{30}$$

where A_{ij}, B_{ij} and C_{ij} are the transfer functions of the three consecutive blocks of Figure 8. Consequently the block diagram of the system (Figure 9) can be simplified to the configuration depicted in Figure 10.

Effect of Location and Magnitude of Barrier on Dynamic System Output

In the time-domain twin-experiments we used flow rates in the injector and pressures in the producer as inputs, and flow rates in the producer as outputs. Therefore, can simplify the configuration depicted in Figure 10 in such a way that the single output of our system, $\Theta(\xi_4, s)$, is influenced by two inputs: $\Theta(\xi_1, s)$ and $\Pi(\xi_4, s)$. Consequently the input-output relation of the system is described by the transfer functions S_{11} and S_{12} only; see Figure 11.

With the aid of equation (26) we can now write an expression for the system output as follows:

$$\Theta(\xi_4,s)=\Theta(\xi_1,s)S_{11}+\Pi(\xi_4,s)S_{12}. \tag{31}$$

Because we used step inputs in the time-domain twin-experiments, the dimensionless form of our inputs in the Laplace domain can be written as

$$\Theta(\xi_1, s) = \frac{1}{s}, \tag{32}$$

$$\Pi(\xi_4, s) = \frac{1}{s}. \tag{33}$$

Table 4—Truth parameter values

Parameters	Magnitude	Unit
ξ_2	0.7	-
ξ_3	0.06	-
ξ_4	0.3	-
α_a, α_c	0.75	-
α_b	0.0025	-

By substituting equation (32) and equation (33) in equation (31) the output of the system can be written as

$$\Theta_{out} = \Theta(\xi_4, s) = \frac{1}{s} S_{11} + \frac{1}{s} S_{12} = \frac{1}{s}(S_{11} + S_{12}). \tag{34}$$

Note that all the variables, and therefore the transfer functions, are dimensionless.

At this stage we can replace s in equation (34) with $j\omega_D$, where j is the imaginary unit and ω_D is dimensionless frequency. Dimensionless sampling frequency is defined according to sampling dimensionless time in our time-domain experiments. This will result in a frequency response description of our system. Now we are able to investigate the effect of location and magnitude of the middle block (the flow barrier) on the output of our system. To perform a sensitivity analysis and a parameter estimation, which are presented in next sections, we define a 'truth' case, with parameters listed in Table 4. The 'truth' parameters are equivalent to the parameters of the time-domain 'truth' case. The analytical 'truth' case is used to generate synthetic measurements for parameter estimation purposes in Section 5.

Effect of Location of a Flow Barrier

In this case we vary the location (ξ_2) of the middle block of the system, while the permeability magnitude of that block is fixed at a small value ($\alpha_b = 0.0025$), and evaluate the corresponding output of the system using equation (34). Figure 12 depicts the amplitude of the system output for different middle block positions at different frequencies. The dashed line in Figure 12 is the amplitude of the system output in the absence of the flow barrier.

As can be seen in Figure 12, the output of the system is quite sensitive to the location of the middle block when it has a small magnitude. In the other words, the location of the low permeable barrier significantly affects the output of our system. Moreover, it can be concluded from Figure 12 that as the barrier location is closer to the producer it has more effect on the output.

Effect of Permeability Magnitude of a Flow Barrier

In this case we vary the permeability magnitude (α_b) of the middle block of the system while its location is fixed ($\xi_2 = 0.7$). Subsequently we evaluate the corresponding output of the system for different values of the middle block's permeability magnitude. Figure 13 depicts the frequency response for these cases. Dashed line in Figure 13 is the amplitude of the system output in the absence of the flow barrier.

It can be clearly seen that as the permeability magnitude of the middle block increases i.e., as the resistance to flow decreases, the output of the system becomes less sensitive to the magnitude variations.

Parameter Estimation in the Frequency Domain

In this section we try to estimate uncertain parameters using frequency responses obtained from the transfer function of the system. In this study the location (ξ_2) and magnitude (α_b) of the middle block are considered as unknown parameters; see Figure 8. We try to estimate these parameters by minimizing a mismatch objective function defined as

$$J = \left(\boldsymbol{\Theta}_{observed} - \boldsymbol{\Theta}_{out}\right)^T \mathbf{P}_{\boldsymbol{\Theta}}^{-1} \left(\boldsymbol{\Theta}_{observed} - \boldsymbol{\Theta}_{out}\right), \tag{35}$$

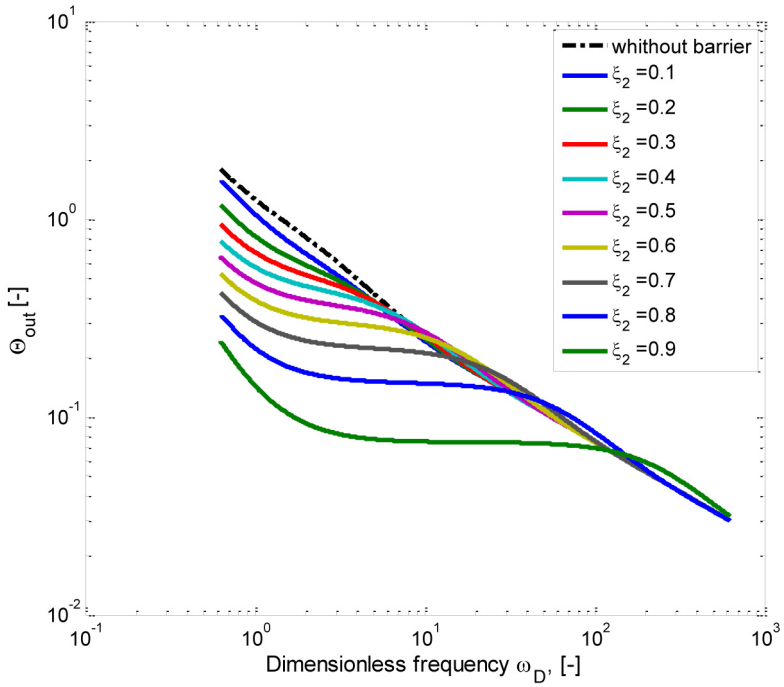

Figure 12—Amplitude of system output for different barrier position and a fixed low barrier permeability magnitude.

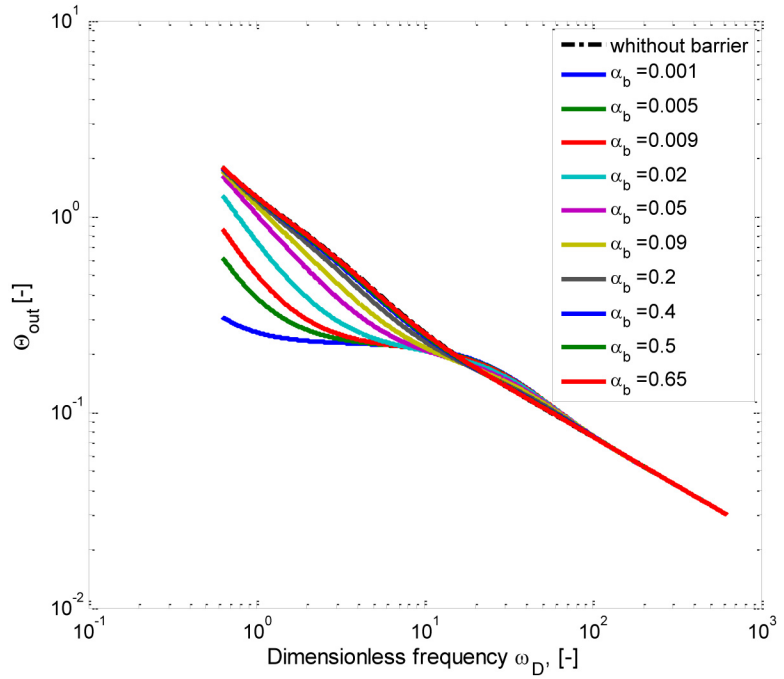

Figure 13—Amplitude of system output for different barrier permeability magnitude and fixed location.

where $\Theta_{observed}$ is the 'truth' output vector, which is generated using 'truth' parameters and equation (34) at different frequencies by replacing s with $j\omega$. Vector Θ_{out} is the simulated output. The starting model parameters are identical to the 'truth' parameters except for the middle block location and magnitude. $\mathbf{P}_{\Theta}$ is the measurement error covariance matrix, which is chosen as an identity matrix in this study. Note that the derivative of the objective function can be calculated analytically. Moreover, since the data vectors (observed and model output) consist of complex numbers we can make our data

Table 5—Model parameters for experiment #1

Parameters	Truth value [-]	Starting value [-]	Estimated value [-]
ξ_2	0.7	0.4	0.7
α_b	0.0025	0.75	0.0025

Table 6—Model parameters for experiment #2

Parameters	Truth value [-]	Starting value [-]	Estimated value [-]
ξ_2	0.7	0.4	0.69
α_b	0.0025	0.75	0.0026

real-valued by considering them as 2D data points, i.e. having real and imaginary parts (Blom and Van den Hof, 2010). Following this approach, we define an augmented data vector by stacking the real and imaginary parts of the complex-valued vectors.

Experiment #1: Noise-Free Parameter Estimation

In the first experiment we use noise-free measurements for parameter estimation purposes. Equation (35) is minimized by adjustment of the location and the magnitude of the middle block. The minimization converges in 15 iterations. The truth, starting and estimated parameter values for this experiment are listed in Table 5.

It can be concluded from Table 5, similar to experiment #1 in time-domain, that in case of noise-free measurements we are able to retrieve the location and the magnitude of a low-perm barrier with 100% accuracy.

Noise Effect on Estimation of Location and Magnitude of a Low-Permeable Barrier

In presence of noise, equation (34) can be written as:

$$\Theta_{out} = \frac{1}{j\omega}\left(S_{11} + S_{12}\right) + v, \tag{36}$$

where v represents noise in the frequency domain. If we assume to have Gaussian white noise in the time-domain, which is the case in our time-domain examples, and considering that the Fourier transform of white noise is white noise, we can use a Fourier transform to convert noise from the time domain into the frequency domain.

Experiment #2: High Signal to Noise Ratio In this experiment we generate white noise from the same distribution as used in section 2.4 for the high signal to noise ratio experiment in the time domain, and use a Fourier transform to transform the noise to the frequency domain. Subsequently, we perform parameter estimation based on this noisy data. The minimization converges in 14 iterations. The truth, starting and estimated parameter values for this experiment are listed in Table 6.

It can be concluded from Table 6, similar to the experiment #2 in the time domain, that for a low amount of noise the location and the magnitude of the low perm barrier can be still retrieved with an acceptable accuracy.

Experiment #3: Low Signal to Noise Ratio In this experiment we increase the amount of noise in the data. Noise is generated from the same distribution as used in section 2.5 for the low signal to noise ratio experiment in the time domain. A Fourier transform is used to transform the noise into the frequency-domain. Subsequently, we perform parameter estimation based on this noisy data. The minimization converges in 11 iterations. The truth, starting and estimated parameter values for this experiment are listed in Table 7.

Table 7—Model parameters for experiment #3

Parameters	Truth value [-]	Starting value [-]	Estimated value [-]
ξ_2	0.7	0.4	0.74
α_b	0.0025	0.75	1.02E-5

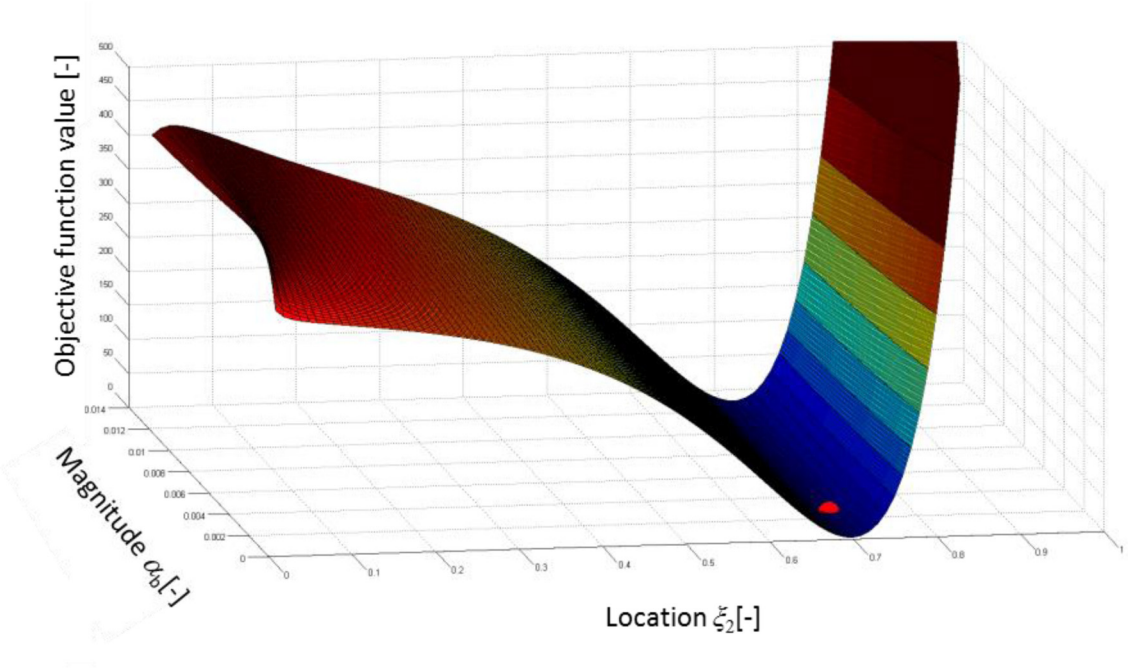

Figure 14—Objective function space. The red dot indicates the minimum.

It can be interpreted from Table 6 and Table 7, that as the noise increases, the accuracy of the estimation of the magnitude parameter becomes worse while the location of the barrier is still accurate. Also these results confirm our twin experiment results in the time domain.

Visualization of the Objective Function

In this section we consider the objective function, expressed in equation (35), which is a function of transfer functions S_{11} and S_{12} and plot it as a function of our two uncertain parameters (location and magnitude of the barrier) in an attempt to visualize the objective function shape and its spatial dependence on the two parameters. Figure 14 depicts the objective function surface in the two-variable space. The red dot in the Figure 14 indicates the minimum of the objective function ('truth' parameters).

If we zoom in on the vicinity of the minimum of Figure 14, we observe that the surface displays a slope in the α_b direction, see Figure 15.

Figure 14 and Figure 15 clearly show that our objective function is more sensitive to the barrier location than to the barrier magnitude, which means that, for the presently chosen input-output configuration and input signals, the barrier location has a higher probability to be estimated correctly from noisy data than the permeability magnitude. This behavior was indeed observed in our parameter estimation results when the amount of noise in the data was increased.

Discussion and Conclusions

The time-domain examples presented in our paper are based on experimental results for a model in which only permeabilities are parameterized, while the frequency domain examples use a model where a

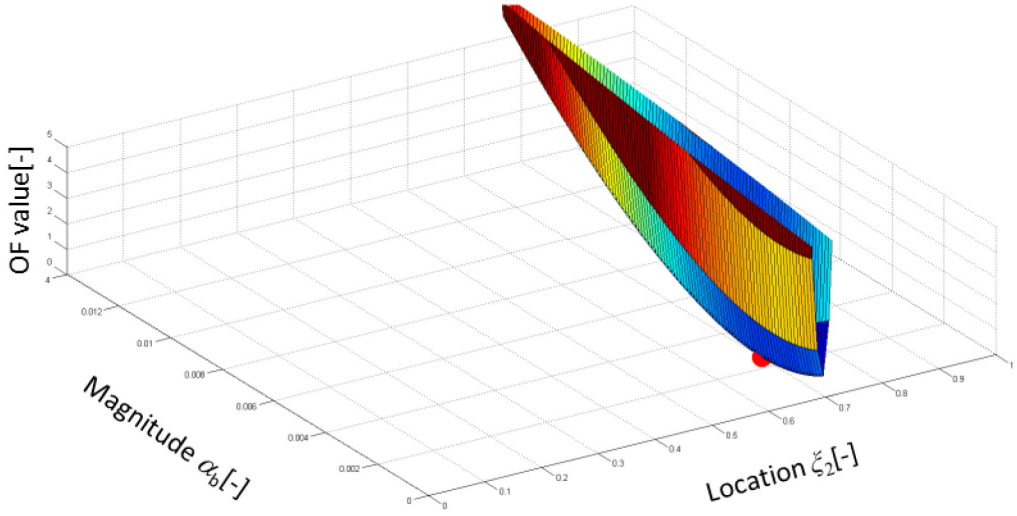

Figure 15—Zoomed in objective function space. The red dot indicates the minimum.

structured physics-based approach is applied in terms of location of the barrier, and magnitude of its permeability. In this sense the frequency domain approach uses more prior knowledge (the barrier is parameterized) than the first (where all permeabilities are estimated separately).

Secondly the first approach is really experiment-driven, while the second approach has to the capacity to say something about identifiability independent of the particular experimental data that is used. Moreover, the frequency domain approach could be used to analyze in which particular frequency region the sensitivity of the parameters is largest, and to design an experiment by picking, e.g., a sinusoidal signal of that (maximum sensitive) frequency. We intend to address these aspects in future research.

In this study we have investigated the possibility of detecting the location and the magnitude of flow barriers in a 1D reservoir for slightly compressible single-phase flow from the observations (outputs) under different noise conditions. To this end we have conducted different twin-experiments in the time domain and the frequency domain. For the latter we have developed an analytical expression for the dynamical characteristics of the system as a function of system properties based on a transfer function formalism in the form of bilaterally coupled porous media models. We conclude that:

- The frequency-domain analytical solution makes it possible to investigate the effect of different parameters on the dynamic behavior of the system.
- It is possible to estimate location and magnitude of a flow barrier from noise-free measurements in slightly compressible single-phase flow.
- When the noise level in the data is increased, the location of the barrier remains relatively more identifiable than its permeability magnitude.
- The presence of noise in the data results in unrealistic permeability magnitude estimates.
- Visualization of the objective function space in the frequency-domain illustrates that the dynamic output of our system is more sensitive to the barrier location than to barrier magnitude.

Nomenclature

$\mathbf{d}$	=	vector of measured data (flow rates), $L^3\ t^{-1}$, m^3/s
$\mathbf{y}$	=	vector of simulated data (flow rates), $L^3\ t^{-1}$, m^3/s
$\mathbf{m}$	=	vector of unknown model parameters (permeability), L^2, m^2
$\mathbf{P}_d$	=	measurement error correlation matrix, $L^6\ t^{-2}$, m^6/s^2
J	=	mismatch objective function, dimensionless
p	=	pressure, $L^{-1}m\ t^{-2}$, Pa

t = time, t, s
x = location, L, m
k = permeability, L^2, m^2
μ = viscosity, $L^{-1}m\ t^{-1}$, Pa.s
c_t = total compressibility, $Lm^{-1}\ t^2$, Pa^{-1}
φ = porosity (dimensionless)
A = surface area, L^2, m^2
L = total length of the domain, L, m
$\hat{p}$ = pressure at the outlet boundary, $L^{-1}m\ t^{-2}$, Pa
$\hat{q}$ = flow rate at the inlet boundary, $L^3\ t^{-1}$, m^3/s
η = hydraulic diffusivity, L^2t^{-1}, m^2/s
ξ = dimensionless length
π = dimensionless pressure
θ = dimensionless flow rate
τ = dimensionless time
α = dimensionless permeability magnitude
s = Laplace variable
ω_D = dimensionless frequency
Π = Laplace domain dimensionless pressure
Θ = Laplace domain dimensionless flow rate
A_{ij} = transfer functions for block A, dimensionless
B_{ij} = transfer functions for block B, dimensionless
C_{ij} = transfer functions for block C, dimensionless
S_{ij} = transfer functions for entire system, dimensionless
$\Theta_{observed}$ = augmented vector of measured data in frequency domain, dimensionless
Θ_{out} = augmented vector of simulated data in frequency domain, dimensionless

Acknowledgement

This research was carried out within the context of the Recovery Factory project at TU Delft, sponsored by Shell Global Solutions International.

References

Ahn, S. and Horne, R. N. 2010. Estimating Permeability Distributions From Pressure Pulse Testing. Paper SPE-134391-MS presented at the SPE Annual Technical Conference and Exhibition, Florence, Italy, DOI: 10.2118/134391-ms.

Blom, R. S. and Van den Hof, P. M. 2010. Multivariable frequency domain identification using IV-based linear regression. Paper presented at the Decision and Control (CDC), DOI: 10.1109/CDC.2010.5717297.

Dogru, A. H., Dixon, T. N. and Edgar, T. F. 1977. Confidence Limits on the Parameters and Predictions of Slightly Compressible, Single-Phase Reservoirs. *SPEJ.* **17** (01): 42–56. DOI: 10.2118/4983-pa.

Grader, A. S. and Horne, R. N. 1988. Interference Testing: Detecting a Circular Impermeable or Compressible Subregion. *SPEFE.* **3**(02): 420–428. DOI: 10.2118/15585-pa.

Joosten, G. J. P., Altintas, A. and Sousa, P. D. 2011. Practical and Operational Use of Assisted History Matching and Model-Based Optimisation in the Salym Field. Paper SPE-146697-MS presented at the SPE Annual Technical Conference and Exhibition, Denver, Colorado, USA, 30 October-2 November 2011. DOI: 10.2118/146697-ms

Kahrobaei, S., Mansoori, M., Joosten, G. J. P., Van den Hof, P. M. J. and Jansen, J. D. 2014. Hidden Information in Ill-posed Inverse Problems. Paper presented at the 14th European Conference on the Mathematics of Oil recovery (ECMOR XIV), Catania, Italy. DOI: 10.3997/2214-4609.20141825.

Kraaijevanger, J. F. B. M., Egberts, P. J. P., Valstar, J. R. and Buurman, H. W. 2007. Optimal Waterflood Design Using the Adjoint Method. Paper SPE-105764-MS presented at the SPE Reservoir Simulation Symposium, Houston, USA, 26-28 February. DOI: 10.2118/105764-ms.

Oliver, D. S., Reynolds, A. C. and Liu, N. 2008. *Inverse theory for petroleum reservoir characterization and history matching*. Cambridge University Press.

Shah, P. C., Gavalas, G. R. and Seinfeld, J. H. 1978. Error Analysis in History Matching: The Optimum Level of Parameterization. *SPEJ.* **18** (3): 219–228. DOI: 10.2118/6508-pa.

Stallman, R. 1952. *Nonequilibrium type curves modified for two-well systems*. US Department of the Interior, Geological Survey, Water Resources Division, Ground Water Branch.

Van Doren, J. F. M. (2010). *Model structure analysis for model-based operation of petroleum reservoirs*. PhD dissertation. Delft University of Technology. The Netherlands.

Van Doren, J. F. M., Van den Hof, P. M. J., Jansen, J. D. and Bosgra, O. H. 2008. Determining identifiable parameterizations for large-scale physical models in reservoir engineering. Paper presented at the Proceedings of the 17th IFAC World Congress, Seoul.

Watson, A. T., Gavalas, G. R. and Seinfeld, J. H. 1984. Identifiability of Estimates of Two-Phase Reservoir Properties in History Matching. *SPEJ.* **24**(06): 697–706. DOI: 10.2118/12579-pa.

Yaxley, L. M. 1987. Effect of a Partially Communicating Fault on Transient Pressure Behavior. *SPEFE*. **2**(04): 590–598. DOI: 10.2118/14311-pa.

Zandvliet, M. J., Van Doren, J. F. M., Bosgra, O. H., Jansen, J. D. and Van den Hof, P. M. J. 2008. Controllability, observability and identifiability in single-phase porous media flow. *Computational Geosciences.* **12** (4): 605–622. DOI: 10.1007/s10596-008-9100-3.